

## Assessment of turbulence modeling for gas flow in two-dimensional convergent–divergent rocket nozzle

A. Balabel, A.M. Hegab, M. Nasr, Samy M. El-Behery \*

Mechanical Power Engineering Department, Faculty of Engineering, Menoufya University, Shebin El-Kom, Egypt

### ARTICLE INFO

#### Article history:

Received 2 August 2010

Received in revised form 22 December 2010

Accepted 11 January 2011

Available online 18 January 2011

#### Keywords:

Numerical modeling

Compressible flow

Turbulence models

Shock wave

Rocket nozzles

### ABSTRACT

In the present study, the turbulent gas flow dynamics in a two-dimensional convergent–divergent rocket nozzle is numerically predicted and the associated physical phenomena are investigated for various operating conditions. The nozzle is assumed to have impermeable and adiabatic walls with a flow straightener in the upstream side and is connected to a plenum surrounding the nozzle geometry and extended in the downstream direction. In this integrated component model, the inlet flow is assumed a two-dimensional, steady, compressible, turbulent and subsonic. The physics based mathematical model of the considered flow consists of conservation of mass, momentum and energy equations subject to appropriate boundary conditions as defined by the physical problem stated above. The system of the governing equations with turbulent effects is solved numerically using different turbulence models to demonstrate their numerical accuracy in predicting the characteristics of turbulent gas flow in such complex geometry. The performance of the different turbulence models adopted has been assessed by comparing the obtained results of the static wall pressure and the shock position with the available experimental and numerical data. The dimensionless shear stress at the nozzle wall and the separation point are also computed and the flow field is illustrated. The various implemented turbulence models have shown different behavior of the turbulent characteristics. However, the shear-stress transport (SST)  $k-\omega$  model exhibits the best overall agreement with the experimental measurements. In general, the proposed numerical procedure applied in the present paper shows good capability in predicting the physical phenomena and the flow characteristics encountered in such kinds of complex turbulent flow.

© 2011 Elsevier Inc. All rights reserved.

### 1. Introduction

The numerical solution of turbulent compressible flows in nozzles is a challenge problem in fluid dynamics applications. Recently, extensive studies have been devoted to understand the fluid dynamics phenomena in rocket motor nozzles. The increased attention is due to a host of technological applications. One example of an important problem is the exhaust gas from jet engines and solid propellant rocket motor. The internal nozzle flow development of a solid rocket plays an essential role both in nozzle design and performance. In particular, the mean velocity field, the axial pressure distribution and the turbulence characteristics have a strong and direct impact on many physical processes occurring within the nozzle. The flow behavior inside the combustion chamber of a rocket plays a key role in both motor design and operation. The majority of the previous studies on the rocket motors have involved the investigations of a nozzleless rocket motor to study the applicability of turbulence models and a DNS analysis to this type of flows [1]. However, in real solid rocket motor, both the

\* Corresponding author. Tel.: +20102292318; fax: +20482235695.

E-mail address: [s\\_elbehery@yahoo.com](mailto:s_elbehery@yahoo.com) (S.M. El-Behery).

chamber and nozzle geometries have significant effects on the overall performance. The combustion chamber-nozzle configuration can affect the relationship between the propellant burning rate transients and the co-existing acoustic waves [2,3].

A full treatment of such problems includes the modeling and resolution of complex physical and chemical phenomena which occurs during the solid propellant combustion process. These models are characterized by extremely diverse length and time scales, complex interfaces, reactive, turbulent, and multiphase flows. These complexities are still a big challenge to perform the whole system simulation. Therefore, many investigations have been directed to model, design and test of solid rocket nozzles aiming to a better nozzle performance, e.g. [4,5]. The main conclusion of such investigations was the important effects resulting from the addition of a divergent section to the convergent nozzle. The divergent section provided further expansion of the flow to supersonic conditions at the nozzle exit and resulted in an increase in momentum thrust. However the convergent-divergent (CD) nozzles often incorporate variable geometry to maintain high performance over a wide range of operating conditions. For best efficiency, the required nozzle area ratios are much higher at supersonic flows than subsonic flows. All propulsion systems with CD nozzles may experience a development of diamond pattern occurs downstream from the nozzle which results from expansion and compression waves according to under- or over-predicted regime. However, propulsion systems which have the advantage of variable geometry nozzles operate closer to design conditions than those with fixed geometry nozzles.

Generally, the propulsive force provided by a rocket nozzle is a function of many parameters such as exit to throat area ratio, type of fuel and oxidizer used and the real chamber pressure to the outside one. In addition, a reliable separation model is needed for accurate prediction of the side-loads experienced during startup and shutdown of the engine. A better understanding of flow separation phenomena in over-expanded rocket nozzle could lead to better prevention or even control of flow separation. Moreover, the advancement of exhaust nozzle technology has essential and great effect on the development of gas turbine engines and solid rocket motors.

Several studies for the flow in the rocket nozzle are reviewed and presented. The majority of these investigations are focused on the formation and transportation of shock wave inside a convergent-divergent nozzle and its contribution to the instability of the separation shear layers. When a supersonic nozzle is operated at pressure ratio below its design point, a shock forms inside the nozzle and the flow downstream of the shock separates from the nozzle wall. Numerous past studies have thoroughly investigated supersonic flow separation in over-expanded nozzles [6–14]. A paramount issue is the prediction of the separation location and the separation pressure ratio is defined as the ratio of the pressure just ahead of separation to the ambient pressure.

Although there is a large amount of studies concerning the flow separation in CD nozzles over a wide range of nozzle pressure ratio (NPRs), the detailed investigation on separation flow mechanism is less matured. It seems that this phenomenon is very basic, even though it remains poorly understood. Most of available publications are concentrated on prediction of separation location. Moreover, several researches have investigated the shock structure in over-expanded CD nozzles. In both cases, a high degree of accuracy is required in order to predict the thrust coefficient adequately. The importance of the thrust coefficient in avoiding booms in takeoff can be seen in [15].

The computational studies of the flow field through CD nozzles are based on the solution of the time-dependent Reynolds averaged Navier–Stokes (RANS) equations and the implementation of an appropriate turbulence model for closure of the RANS equations. The governing equations are solved in generalized coordinates and in conservative form. The previous numerical studies have assessed the accuracy of the turbulence model for predicting the flow field and the thrust performance. In general, the turbulence model performance in the flow regions dominated by strong pressure gradients and complex secondary flows can be considered as the most likely culprit for the discrepancies observed between the numerical simulations and the experimental measurements.

Several turbulence models can be used for the computational study ranging from an algebraic to linear and nonlinear two-equation turbulence models. An algebraic model is accurate for simple viscous flows because the turbulent viscosity is determined by a local function. The two-equation turbulence model with second-order closure is used to model more complex viscous flow features such as shear layer and regions of separated flow. The implementation of non-linear eddy viscosity turbulence models is another important topic in the recent modeling of turbulent flow. The non-linear turbulence models have proved their capability to predict the reattaching turbulent shear flow in asymmetric divergent channel in our previous research [16]. However, numerical stability is often problematic and often small time step is required for stability. The same problem can be seen by using the Reynolds-stress transport models in complex flows.

This state of affairs leaves methods that are rely on RANS equations as the most promising alternative for practical engineering computations. Recently, RANS modeling is used to predict most of complex viscous flows feature encountered in engineering applications such as shear layers and regions of separated flow in conjunction with near wall function or damping function to adjust the turbulent viscosity near the solid walls. Even in two-phase flows, the RANS modeling can be used in a wide range [17]. Although, a complete agreement with experiments is not achieved, these models succeeded in resolving complex features of both the mean flow and turbulence field. Our research group has tested, in parallel research, five different turbulence models for predicting turbulence in porous channel with constant mass injection [18]. The obtained results showed that the two-equation  $k-\varepsilon$  turbulence model can be extended and used in such complex flows.

Recently, five turbulence models have been assessed in terms of their effects on the agreement between the experimental centerline pressure distribution and the 2D computational results at over-expanded conditions [19]. The turbulence models considered are the algebraic models of Baldwin–Lomax, RNG, the one equation model of Baldwin–Barth and the two-equation  $k-\varepsilon$  and  $k-\omega$  models of Chien and Wilcox. Their results indicated that both the shock location and pressure level behind the

shock are strongly affected by the turbulence model, where agreement with experimental data has been obtained only up to the point of shock and then varied significantly in the predicted shock location and pressure level behind the shock. In the 3D simulations, the computed results are very sensitive to the turbulence models and the two-equation models could predict good results. In addition, they demonstrated that the interactions created through external flow entrainment, and their effects on surface pressure distribution, might not be adequately simulated if only the nozzle interior domain is considered.

The two-equation  $k-\omega$  turbulence model in conservation law form and general curvilinear coordinate in Ref. [20] is used to predict the surface pressure distribution and internal thrust coefficient of a two-dimensional CD nozzle. In comparison with the results obtained using Spalart–Allmaras turbulence model, study of Ref. [21] confirmed the importance of the turbulence model in producing realistically or unrealistically numerical results.

Although of the wide application of several turbulence models in a variety of flow fields, it is yet remains a widely debated subject. Even though some experiments and analysis have shown that the motion of the shock wave can be affected by turbulent fluctuations in the attached boundary layer in upstream direction [22], it would seem that in general, the initial perturbations comes from fluctuation in the downstream separated flow [23]. Through the measurements of the wall pressure spectra near the recirculation regions, two spectral lower and higher frequency bumps have been observed [24]. This has been attributed to the finite length of the larger and smaller recirculation zones, respectively.

Because the motivation behind our present investigation is to demonstrate a numerical method that can predict the physical phenomena of turbulent gas flow in a solid rocket nozzle with an appropriate turbulence model, our primary focus is not the source of the shock unsteadiness but rather the impact of the turbulence model adopted on the shock position and movement on the flow downstream and its contribution to the instability of the separation shear layer. The general prediction method for heat and mass transfer proposed by Patankar [25] was used to obtain the numerical solution of the two-dimensional compressible Reynolds averaged Navier–Stokes (RANS) equations. Several turbulence models; namely the standard  $k-\varepsilon$  (STD) model [26], the extended  $k-\varepsilon$  (ETD) model [27], the  $k-\varepsilon-v^2-f(v^2-f-1)$  model [28], realizable  $k-\varepsilon-v^2-f(v^2-f-2)$  model [29], shear-stress transport (SST)  $k-\omega$  model [30] and Reynolds stress model (RSM) [31] are used in the present numerical simulation in predicting the internal nozzle flow over a wide rang of nozzle pressure ratios. It should be pointed out that, the extended  $k-\varepsilon$  (ETD), the  $k-\varepsilon-v^2-f(v^2-f-1)$  and realizable  $k-\varepsilon-v^2-f(v^2-f-2)$  turbulence models have been implemented by the authors in the computational fluid dynamics code, FLUENT 6.3 [31]. The comparison with the available experimental data is used to asses the accuracy of the turbulence model adopted.

Recently, there is an increased interest in two-dimensional convergent–divergent nozzles as a result of the advantages they offer over axisymmetric configurations for supersonic transport. These include higher performance, reduced after-body drag, easier integration with airframes, and large mechanical area excursion capabilities. However, the performance of these nozzles can suffer at off-design conditions when the large nozzle area ratio reductions required under certain operating conditions. Moreover, the previous experimental measurements have proved that the gas expands faster in a non-circular nozzle shape. Consequently, the numerical prediction of turbulent flow in two-dimensional CD is the subject of the most recent studies to predict off-design performance with a high degree of accuracy. However, unlike axisymmetric nozzles for rocket engines, the prediction of two-dimensional CD nozzle performance at overexpanded conditions is a big challenge, in light of the complex three-dimensional phenomena associated with shock-boundary layer interactions and flow separation over the endwalls [19].

The purpose of the present investigation is to assess the computational results obtained for two-dimensional CD nozzles using different turbulence models. The two-dimensional CD nozzle tested under static conditions by Hunter [8] was selected for the numerical assessment because the large number of pressure taps gave a better prediction of the shock location. The computational domain consists of a flow straightener followed by the convergent–divergent nozzle which connected to a plenum surrounding the nozzle geometry and extended in the downstream direction.

## 2. Computational code and procedure

The finite volume solver, FLUENT 6.3, is used to obtain the numerical solution of the two-dimensional compressible Reynolds averaged Navier–Stokes (RANS) equations in connection with six turbulence models for closure of the RANS equations. The discretized equations, along with the initial condition and boundary conditions, were solved using the segregated solution method. Using the segregated solver, the conservation of mass and momentum were solved sequentially and a pressure-correction equation was used to ensure the conservation of momentum and the conservation of mass (continuity equation). Several turbulence models, i.e. the standard  $k-\varepsilon$  model, the extended  $k-\varepsilon$  model, shear-stress transport  $k-\omega$  model, RSM,  $v^2-f$  and the realizable  $v^2-f$  model are tested. The extended  $k-\varepsilon$  model differs from the standard  $k-\varepsilon$  model in its constant and it has an additional source term in the  $\varepsilon$  equation. This model was implemented in the code by adjusting the standard  $k-\varepsilon$  model constants and by defining the additional source term using User Defined Functions (UDF). Moreover, the four equation turbulence  $v^2-f$  models are implemented using User Defined Scalars (UDS) along with UDF.

### 2.1. The governing equations

The governing equations consist of the continuity equation and the Reynolds-averaged governing equations for steady compressible turbulent flow coupled with the equation of state,  $p = \rho RT$ . The system of the governing equations can be described as follows:

The continuity equation:

$$\frac{\partial}{\partial x_i} (\rho u_i) = 0. \quad (1)$$

RANS equations:

$$\frac{\partial}{\partial x_j} (\rho u_i u_j) = -\frac{\partial p}{\partial x_i} + \frac{\partial}{\partial x_j} \left[ \mu \left( \frac{\partial u_i}{\partial x_j} + \frac{\partial u_j}{\partial x_i} - \frac{2}{3} \delta_{ij} \frac{\partial u_l}{\partial x_l} \right) \right] + \frac{\partial}{\partial x_j} (-\rho \bar{u}_i' \bar{u}_j'). \quad (2)$$

Energy equations:

$$\frac{\partial}{\partial t} (\rho E) + \frac{\partial}{\partial x_i} [u_i (\rho E + p)] = \frac{\partial}{\partial x_j} \left( \left( k + \frac{C_p \mu_t}{0.85} \right) \frac{\partial T}{\partial x_j} + u_i (-\rho \bar{u}_i' \bar{u}_j') \right). \quad (3)$$

where  $u$  denotes mean quantities and the  $u'$  fluctuating or turbulence quantities,  $\rho$  is density,  $p$  is pressure,  $\mu$  is viscosity. The additional fluctuating quantities  $\bar{u}_i' \bar{u}_j'$  are the unknowns turbulent or Reynolds-stress tensors, while  $u_i'$  represents the velocity fluctuation in  $i$ -direction. These equations are not a closed set and turbulence closure is required to model the turbulent or Reynolds-stress tensors.

## 2.2. Turbulence models

Several available turbulence models are employed to predict the flow behavior in the considered physical domain. Most of these models are derived from standard  $k-\varepsilon$  model and vary in complexity and robustness from two equation turbulence models to more elaborated turbulence model. Five turbulence models belongs to the category of eddy viscosity models, while the sixth model, the Reynolds stress model (RSM), is a more general model than those based on the Boussinesq assumption [32]. In this model, a separate transport equation for each component of the Reynolds stresses is solved.

### 2.2.1. Eddy viscosity models (EVM)

In the present paper, five eddy viscosity models are tested and evaluated for the case considered. In these models, the apparent turbulent shearing stresses might be related to the rate of mean strain through an apparent scalar turbulent or "eddy" viscosity. For the general Reynolds stress tensor, the Boussinesq assumption gives:

$$-\rho \bar{u}_i' \bar{u}_j' = \mu_t \left( \frac{\partial u_i}{\partial x_j} + \frac{\partial u_j}{\partial x_i} \right) - \frac{2}{3} \left( \rho k + \mu_t \frac{\partial u_k}{\partial x_k} \right) \delta_{ij}, \quad (4)$$

where  $\delta_{ij}$  is the Kronecker delta function ( $\delta_{ij} = 1$  if  $i = j$  and  $\delta_{ij} = 0$  if  $i \neq j$ ),  $k$  is the turbulent kinetic energy and  $\mu_t$  is the turbulent viscosity. In order to obtain the turbulent viscosity, other transport equations are needed. Theses equations differ from one model to another. The general transport equations for the adopted models are given below, while the different terms and coefficient of the turbulence models adopted are given in Table 1.

**Table 1**  
Coefficient for the adopted turbulence models.

STD $k-\varepsilon$ model	ETD $k-\varepsilon$ model	$\nu^2-f$ model	SST $k-\omega$
$\beta_1$	1	1	0
$\beta_2$	0	0	0.09
$\beta_3$	0	0	0.0828
$\sigma_k$	1	0.75	1
$\sigma_\varepsilon$	1.3	1.15	0
$\sigma_\omega$	0	0	1.168
$P_k$	$2\nu S_{ij} S_{ij}$	$2\nu S_{ij} S_{ij}$	$2\nu S_{ij} S_{ij}$
$S_{ij}$	$0.5(u_{i,xj} + u_{j,xi})$	$0.5(u_{i,xj} + u_{j,xi})$	$0.5(u_{i,xj} + u_{j,xi})$
$P_k^*$	$P_k$	$P_k$	$\text{Min}(P_k, 10\varepsilon)$
$C_{1\varepsilon}$	1.4	1.15	0
$C_{2\varepsilon}$	1.92	1.9	0
$C_{3\varepsilon}$	0	0.25	0
$T$	$k/\varepsilon$	$k/\varepsilon$	$1/\omega$
$\mu_t$	$\rho C_\mu k^2/\varepsilon$	$\rho C_\mu k^2/\varepsilon$	$0.31\rho k/\text{Max}(0.31\omega, F_2(2S_{ij}S_{ij})^{0.5})$
$C_\mu$	0.09	0.09	0
$L$	0	0	0
$F_2$	0	0	$\tanh(D_1)^2$
$D_1$	0	0	$((2k^{0.5}/0.09\omega y), 500\nu/\omega y^2)$
$\gamma_1$	0	0	0.4403
$F_{SST}$	0	0	$2.336(1 - F_1)(1/\omega)(k_{xj}\omega_{xj})$
$F_1$	0	0	$\tanh(D_2)^4$
$D_2$	0	0	$\text{Min}(\text{Max}(D_1, 4.672\rho k/D_3 y^2))$
$D_3$	0	0	$\text{Max}(2.336\rho(1/\omega)(k_{xj}\omega_{xj}), 1 \cdot e^{-10})$

The  $k$ -equation:

$$\frac{\partial}{\partial x_j} (\rho u_j k) = \frac{\partial}{\partial x_j} \left[ \left( \mu + \frac{\mu_t}{\sigma_k} \right) \frac{\partial k}{\partial x_j} \right] + \rho (P_k^* - \beta_1 \varepsilon - \beta_2 k \omega). \quad (5)$$

The  $\varepsilon$ -equation:

$$\frac{\partial}{\partial x_j} (\rho u_j \varepsilon) = \frac{\partial}{\partial x_j} \left[ \left( \mu + \frac{\mu_t}{\sigma_\varepsilon} \right) \frac{\partial \varepsilon}{\partial x_j} \right] + \frac{\rho}{T} \left( C_{1\varepsilon} P_k - C_{2\varepsilon} \varepsilon + C_{3\varepsilon} \frac{P_k^2}{\varepsilon} \right). \quad (6)$$

The  $v^2$ -equation:

$$\frac{\partial}{\partial x_j} (\rho u_j v^2) = \frac{\partial}{\partial x_j} \left[ \left( \mu + \frac{\mu_t}{\sigma_k} \right) \frac{\partial v^2}{\partial x_j} \right] + \rho \left( kf - v^2 \frac{k}{\varepsilon} \right). \quad (7)$$

The  $f$ -equation:

$$L^2 \frac{\partial^2 f}{\partial x_j^2} - f = \frac{1}{T} \left[ (-4.6) \frac{v^2}{k} - \frac{0.8}{3} \right] - 0.3 \frac{P_k}{k}. \quad (8)$$

The  $\omega$ -equation:

$$\frac{\partial}{\partial x_j} (\rho u_j \omega) = \frac{\partial}{\partial x_j} \left[ \left( \mu + \frac{\mu_t}{\sigma_\omega} \right) \frac{\partial \omega}{\partial x_j} \right] + \rho^2 \frac{\gamma_1}{\mu_t} P_k - \rho \beta_3 \omega^2 + F_{SST}. \quad (9)$$

The effect of compressibility on turbulence models is known as “dilatation dissipation”. The considering of compressibility effect enables the prediction of the observed decrease in spreading rate with increasing Mach number for compressible mixing and other free shear layers. The difference between the two  $v^2-f$  models lies on the calculation of time scale,  $T$ . In the first model,  $v^2-f-1$ , the time scale was calculated by:

$$T = \max \left[ \frac{k}{\varepsilon}, 6 \sqrt{\frac{v}{\varepsilon}} \right]. \quad (10)$$

In the second model,  $v^2-f-2$ , realizability constrains on the turbulent time scale was applied. This constrains was originally suggested by Durbin [29]. Sveningsson and Davidson [33] found that application of this constrains with  $f$ -equation can cause numerical problems. The same convergence difficulties are found in the present study. Thus, a converged solution can not be obtained with constrains on  $T$  used with  $f$ -equation, even with first order discretization and low under relaxation factors. Therefore, following the recommendation of Sveningsson and Davidson [33], the realizability constrains are applied to the turbulent viscosity and dissipation rate equations only. The turbulent time scale of  $v^2-f-2$  can be written as:

$$T = \min \left[ \max \left[ \frac{k}{\varepsilon}, 6 \sqrt{\frac{v}{\varepsilon}} \right], \frac{0.6}{\sqrt{3}} \frac{k}{v^2 C_\mu \sqrt{2 S_{ij} S_{ij}}} \right]. \quad (11)$$

### 2.2.2. Reynolds stress model (RSM)

The Reynolds stress model (RSM) is a higher level, elaborated turbulence model. It is usually called a second order closure. This modeling approach originates from [32]. In RSM, the eddy viscosity approach has been discarded and the Reynolds stresses are directly computed. The exact Reynolds stress transport equation accounts for the directional effects of the Reynolds stress fields. Detailed derivations for the closure equations can be found in [31].

### 2.3. Near-wall modeling

In the region near the wall, the gradient of quantities is considerably high and requires fine grids close to the wall to capture the changes of quantities. For complex flows where separation flow and reattachment occur, the conventional logarithmic wall-function proposed by Launder and Spalding [34] becomes less reliable. The non-equilibrium wall-function proposed by Kim and Choudhury [35] is proven to give better predictions since its account the effects of pressure gradient and departure from equilibrium. For the standard  $k-\varepsilon$  model and the extended  $k-\varepsilon$  model, the non-equilibrium wall-function is applied to the wall-adjacent cells, while for  $v^2-f$  models the near-wall turbulence is treated without the use of exponential damping or wall functions. For the SST  $k-\omega$  models, if the *transitional flows option* is enabled in the viscous model panel (shown in the adopted code), low-Reynolds-number variants will be used, and, in that case the near-wall grids have to be very fine to obtain the better results for the near wall modeling. If *transitional flows option* is not active as in the present study, the near wall grids follow a rule of the wall function. The use of a wall function in a computational flow solver allows fewer points to be placed near the walls where these points are typically placed to  $Y^+ = 1$  for a wall integrated grid. In the present study  $Y^+$  changed from 0.8 to 1.1 depending on the nozzle pressure ratio and on the selected turbulence model.

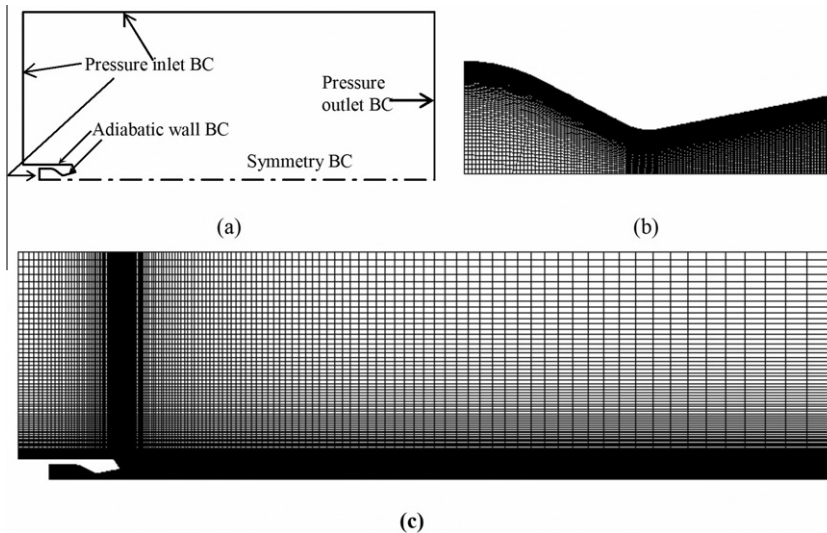


**Fig. 1.** (a) Computational domain, (b) nozzle computational grid and (c) total computational grid.

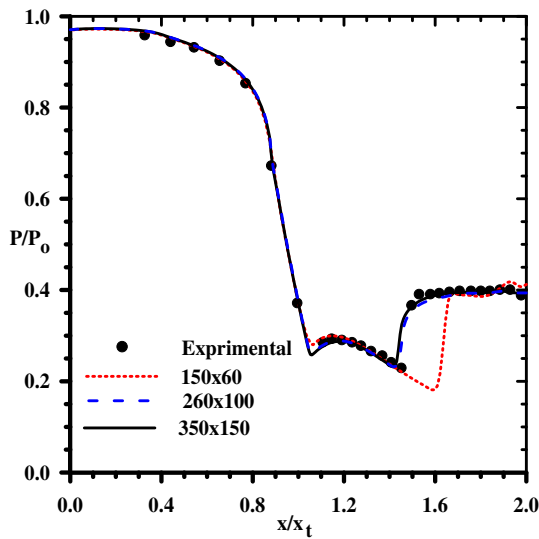


**Fig. 2.** Grid independence study at  $NPR = 2.412$  using SST turbulence model.

#### 2.4. Computational domain and grid generation

A 2-D computational domain with the assigned boundary conditions is shown in Fig. 1a. The selection of the space grid will influence the solution obtained. When using a finer grid, the basic flow structure changes little, but it increases the computational cost greatly. Therefore, the grid chosen represents a compromise between the accuracy and computer time. A grid refinement study was conducted for a nozzle pressure ratio of 2.412. Fig. 2 shows a comparison between predicted pressure distribution using three different meshes and experimental data of [8]. The results are presented for  $150 \times 60$ ,  $260 \times 100$  and  $350 \times 150$  computational grids inside the convergent-divergent nozzle which correspond to a total computational grid (inside and outside the nozzle) of 31,614, 118,592 and 241,538, respectively. The comparison shows that the results obtained using  $260 \times 100$  and  $350 \times 150$  computational grids inside the convergent-divergent nozzle are very close. Therefore, the computations are performed on  $260 \times 100$  to reduce the computational time. In this case, the gird is clustered toward the nozzle wall and the dimensionless wall distance,  $Y^+$  is found to be varied between 0.8 and 1.1 for all the tested cases. The  $260 \times 100$  computational girds inside the nozzle is presented in Fig. 1b, while the total computational grid is shown in Fig. 1c.

## 2.5. Boundary conditions

The assigned boundary conditions, as prescribed in Fig. 1a are declared as follows. The pressure outlet boundary conditions are specified on the right boundaries, which require the specification of a static (gauge) pressure at the outlet boundary when the flow is subsonic. Should the flow become locally supersonic, the specified pressure will no longer be used and the pressure will be extrapolated from the flow in the interior. All other flow quantities are extrapolated from the interior.

Ambient pressure and temperature conditions are considered as total conditions at the top and left external boundaries, while stagnation conditions are specified at the inlet to duct upstream of the nozzle. In addition, a static pressure was specified at the duct inlet to start the solution. Symmetry boundary conditions are applied at the symmetry plane, and no-slip conditions at the walls.

## 3. Validations

The validations of the turbulence models in the present investigation are based on the comparison of the static pressure on the upper nozzle surface with the experimental measurements data [8] at different nozzle pressure ratio (NPR). The NPR is defined as the ratio of the total (or stagnation) pressure at the nozzle inlet  $P_o$  and the ambient pressure  $P_a$ . The exhaust flow pattern depends on whether the flow is under-expanded or over-expanded [22]. Because of the external exhaust flow

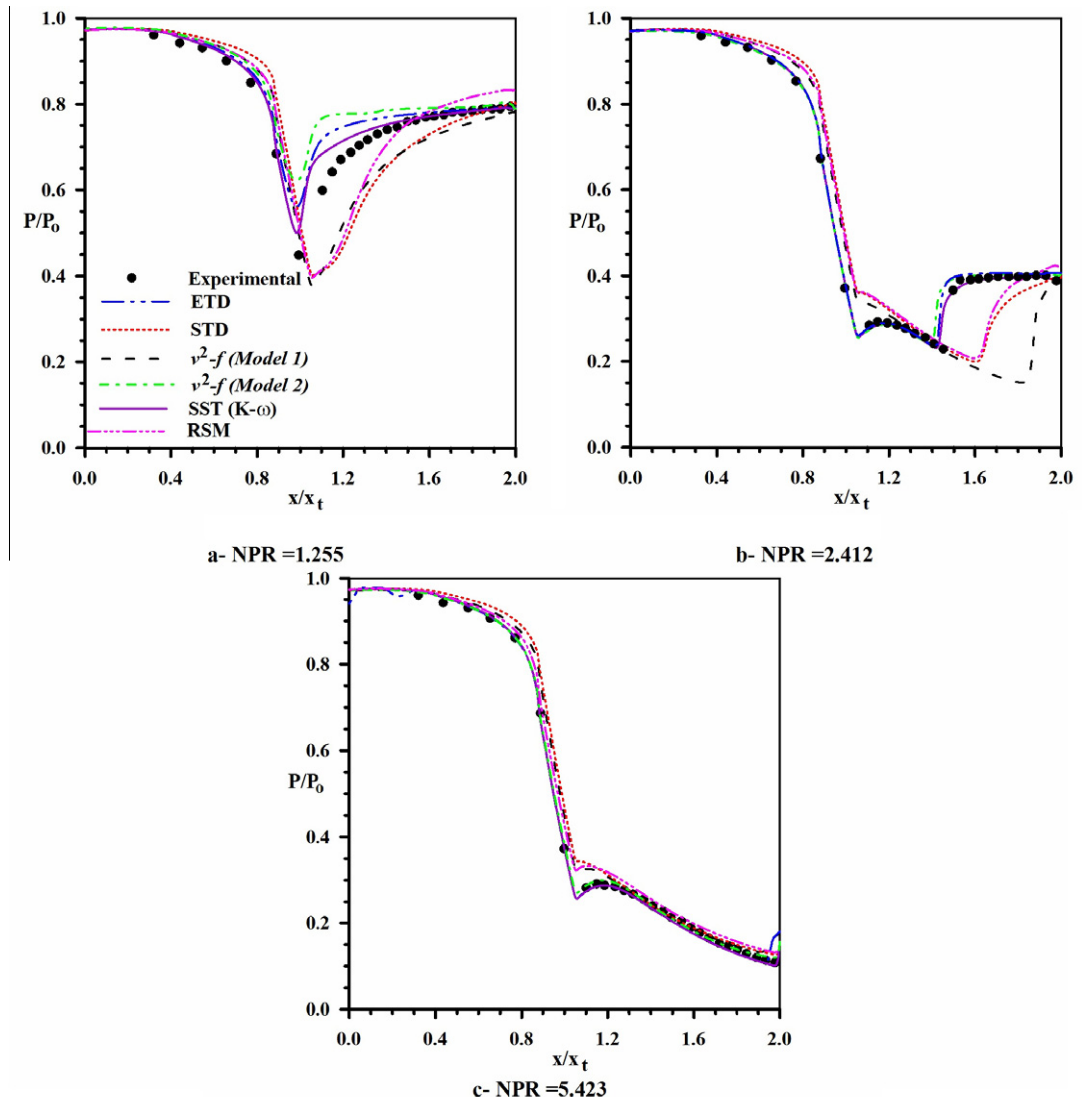


**Fig. 3.** Comparison of the present results with the experimental measurements [8] for different turbulence models.

expansion has a free (ambient-exhaust) boundary, the nozzle performance characteristics is a function of NPR, Mach number  $M$  and the attack angle. However, in the static (wind-off) investigation, the internal performance parameters depend on NPR only. Moreover, the flow pattern, shock structure, flow separation and shear layer detachment are strongly affected by the NPR.

In the present paper, a wide range of NPR is considered. Fig. 3 shows the comparison between the computational results obtained using the six turbulence models presented earlier (cf. Section 2) and the experimental measurements found in [8]. The static wall pressure is normalized using the stagnation pressure  $P_o$  and plotted against the non-dimensional streamwise location  $x/x_t$ , where  $x_t$  is the streamwise location at nozzle throat. The comparison is carried out for  $\text{NPR} = 1.255, 2.412$  and  $5.423$ .

For low  $\text{NPR} = 1.255$ , as shown in Fig. 3a, the pressure fields indicate a weak shock near the geometric throat and the internal flow downstream of the shock is over-expanded and appears to recover smoothly to the ambient pressure. By comparing the capability of the used turbulence models in predicting the shock formation and position, it is found that the numerical predictions using the SST turbulence model show close agreement with the experimental measurements. In contrast, the ETD  $v^2-f-2$  turbulence models illustrate over-predicted pressure distribution. However, the RSM, STD and  $v^2-f-1$  turbulence models under-predicted the pressure distribution.

For medium  $\text{NPR} = 2.412$ , shown in Fig. 3b, the shock position nearly approaches the nozzle exit and there is almost no pressure recovery downstream of the shock. This result indicates that the internal flow adjusted itself to the exit conditions by completely detaching past the shock. The SST and  $v^2-f-2$  turbulence models predict the experimental measurements in a good agreement, while the results of the ETD turbulence model could be accepted with some cautions. In contrast, the results of the RSM, STD and  $v^2-f-1$  turbulence models show large deviations from the experimental measurements especially downstream of the shock position.

By increasing the NPR to be about 5.423, as shown in Fig. 3c, the numerical results show that the nozzle is shock free. The pressure downstream of the nozzle throat indicates that the internal flow is found to be independent of the NPR. By comparing the numerical results obtained from the four turbulence models, the SST and  $v^2-f-2$  turbulence models are nearly the more suitable models in predicting the experimental data and the pressure distribution. The ETD turbulence model give also good agreement; however, this model shows a little increase in the wall pressure near the nozzle exit in order to match the prescribed boundary conditions. The success of the ETD turbulence model in this range of NPR may be referred to the shock free internal flow. However, the RSM, STD  $k-\varepsilon$  and  $v^2-f-1$  turbulence models still give over-predicted results in spite of the absence of shock inside the nozzle.

From the above comparison, it is found that the numerical predictions using the SST and  $v^2-f-2$  transport turbulence models show close agreement with the experimental results more than that given by the other turbulence models. The formulation of SST turbulence model in the gradual change from the standard  $k-\omega$  model in the inner region of the boundary layer to a high-Reynolds-number  $k-\varepsilon$  model in the outer part of the boundary layer enables it to capture the shock wave/boundary layer interaction accurately. In addition, the turbulent viscosity is modified to account for the transport effects of the principal turbulent shear stress. The  $v^2-f$  turbulence model incorporates some near-wall turbulence anisotropy as well as non-local pressure-strain effects. Including the realizability constraints on the turbulent time scale greatly enhances the prediction of the model for this particular case. The more complex RSM produces very poor results. In addition, this model requires the greater number of iterations and computational time because it has six additional transport equations for the current 2D problem. Furthermore, a converged solution can not be obtained using second order discretization even if the flow is initiated from a converged solution obtained by other turbulence model. Therefore, first order upwind discretization scheme is applied for RSM. Similar failure of RSM was reported by other researchers when they apply the RSM for separating flow in a diffuser [36,37] and flow subject to streamline curvature [38]. Therefore, the failure of the RSM in the present case is not surprising because it is a more complex flow problem than diffusers and bends. The ETD turbulence model proposed an extra time scale of the production range included in the dissipation rate equation. That pushes the model to perform quite well in the turbulent boundary layer flows. The STD  $k-\varepsilon$  turbulence model needs further improvement to be suitable for the shock wave turbulent boundary layer interaction applications. The  $v^2-f$  turbulence model has two extra transport equations as it compared with the SST turbulence model. Therefore, the computational time is increased by about 20%. Therefore, the SST model is recommended for the simulation of compressible flow through convergent-divergent nozzle.

The success of the SST turbulence models in better prediction of turbulent flow characteristics through convergent-divergent has been also demonstrated by Östlund [39]. However, in the present SST model, the wall function approach is applied, while the SST model of Östlund integrates the flow equations directly up to the wall. Both models are available directly in Fluent. If the transitional flow option is disabled, Fluent activates the high Reynolds number version of SST  $k-\omega$  model which follows the wall function approach. While, if the transitional flow option is enabled, Fluent activates the low Reynolds number version which solves directly up to the wall. The difference between these two models lies in the way of how the model parameters are evaluated. Thus, in the low-Re model some of the model parameters are calculated as a function of the local flow properties, while for high-Re model they are treated as constants, see Ref. [31] for more details. In addition, Menter [40] recommended the use of the SST model with the wall function approach for flow in complex geometries. However, when both models are applied in the present case using the current grid ( $260 \times 100$  computational grids inside the convergent-divergent nozzle), they produce identical results. However, the extra functions included in the low-Re SST model causes strong coupling between flow equations. As a result, the computational time of the low-Re model is greater than that of the high-Re model by about 4%. Comparison between the two model predictions, using the coarser grid ( $150 \times 60$

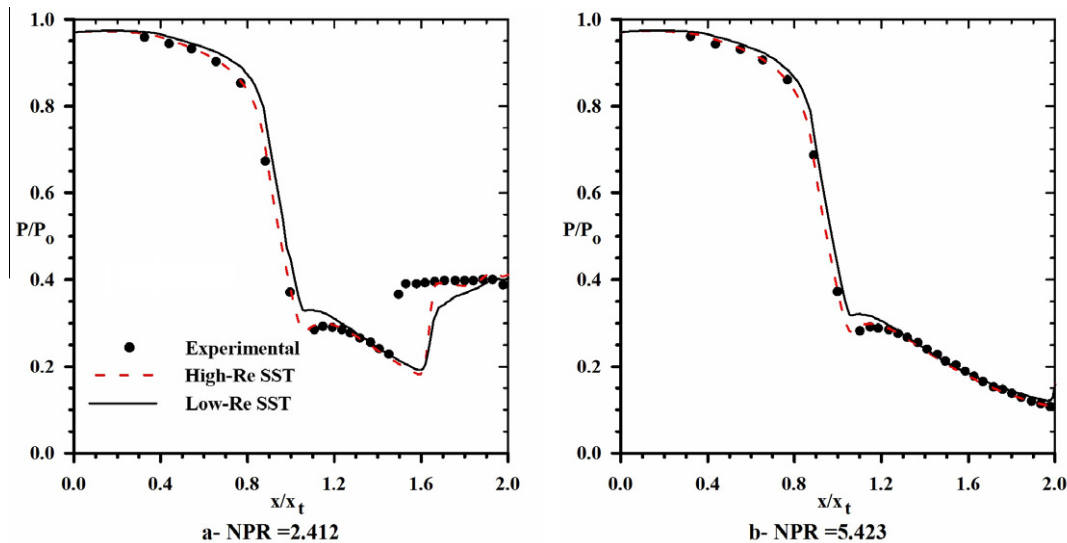


**Fig. 4.** Comparison between low and high Reynolds number SST models using the coarser grids.

computational grids inside the convergent–divergent nozzle) which gives  $Y^+$  between 50 and 80, is presented in Fig. 4. It can be seen from the figure that the high-Re model gives more accurate results at  $NPR = 5.423$  which corresponds to shock-free inside the nozzle. For the cases involving shocks, both models failed to predict the correct shock position when the coarse grid is used. This suggests that the high-Re model can be used in the shock-free cases with relatively coarse mesh with a fair accuracy. However, in the present study the grid resolution is not only controlled by near wall distance but also by the shock wave capturing capabilities and shock wave/boundary layer interactions. Therefore, the high Reynolds number SST model with the wall function approach is recommended in the present study with a fine mesh to predict the shock wave position accurately and to reduce the computational time.

#### 4. Results and discussion

As indicated previously, the SST turbulence model showed the best overall performance in terms of computational time and accuracy. Therefore, in order to provide better understanding of turbulent flow behavior inside the convergent–divergent nozzle, the SST model is applied in the present numerical simulation for turbulent nozzle flow with a wide range of NPRs.

The computed Mach number contours for different NPRs 1.255, 2.412, 2.607, 3.014, 5.423 and 7.03 are plotted in Fig. 5. These contours describe briefly the principal separation phenomena in a symmetric nozzle, Fig. 5a–d. One can see clearly near the wall, the separation shock consists of incident and reflected oblique waves that merge into a Mach stem at the triple point. This is so-called lambda foot of the shock [11,13].

The present results show, for low  $NPR = 1.255$ , a weak normal shock downstream of the nozzle throat with no lambda foot structure evident. However, the results show, for  $NPR = 2.412$ , a nozzle shock with a pronounced lambda foot structure and fully detached separation layer extended from the leading lambda shock in downstream. The separation region formed downstream can be considered as consequence of the adverse pressure gradient through the shock, which forces the incoming boundary layer to separate. The oblique shock structures are of the weak type resulting in low supersonic flow downstream while the flow immediately past the Mach stem is subsonic.

The same results are obtained for subsequent NPRs greater than 2.412, e.g.  $NPR = 2.607$  and 3.014, as shown in Fig. 5c and d. Moreover, the separation shear layers emerged as expansion fans and transmitted across the test section to the opposite shear layer and then reflected again as compression waves. This reflection continues downstream, resulting in a series of expansion and compression waves through the separation region.

By increasing the NPR, the lambda foot is grown significantly, such that the main shock and the trailing lambda foot are located behind the nozzle exit. The nozzle is shock free and the flow is found to be over-expanding externally, as shown in Fig. 5e and f for  $NPR = 5.423$  and 7.03, respectively. Also these figures show multi interaction of compression and rarefaction wave downstream of the nozzle exit. This phenomenon is similar to the supersonic jet behavior.

The above results indicate that the shock location inside the nozzle and the separation point are affected by the NPR. Therefore, a wide range of NPRs has been simulated using the SST turbulence model. The predictions of the shock position as well as the separation point are plotted and compared with the experimental measurements [8], as shown in Fig. 6. The results indicate that by increasing the NPR, the shock position as well as the separation point move downstream. By increasing the NPR to be about five, it is found that the shock location does not change nearby the nozzle exit.

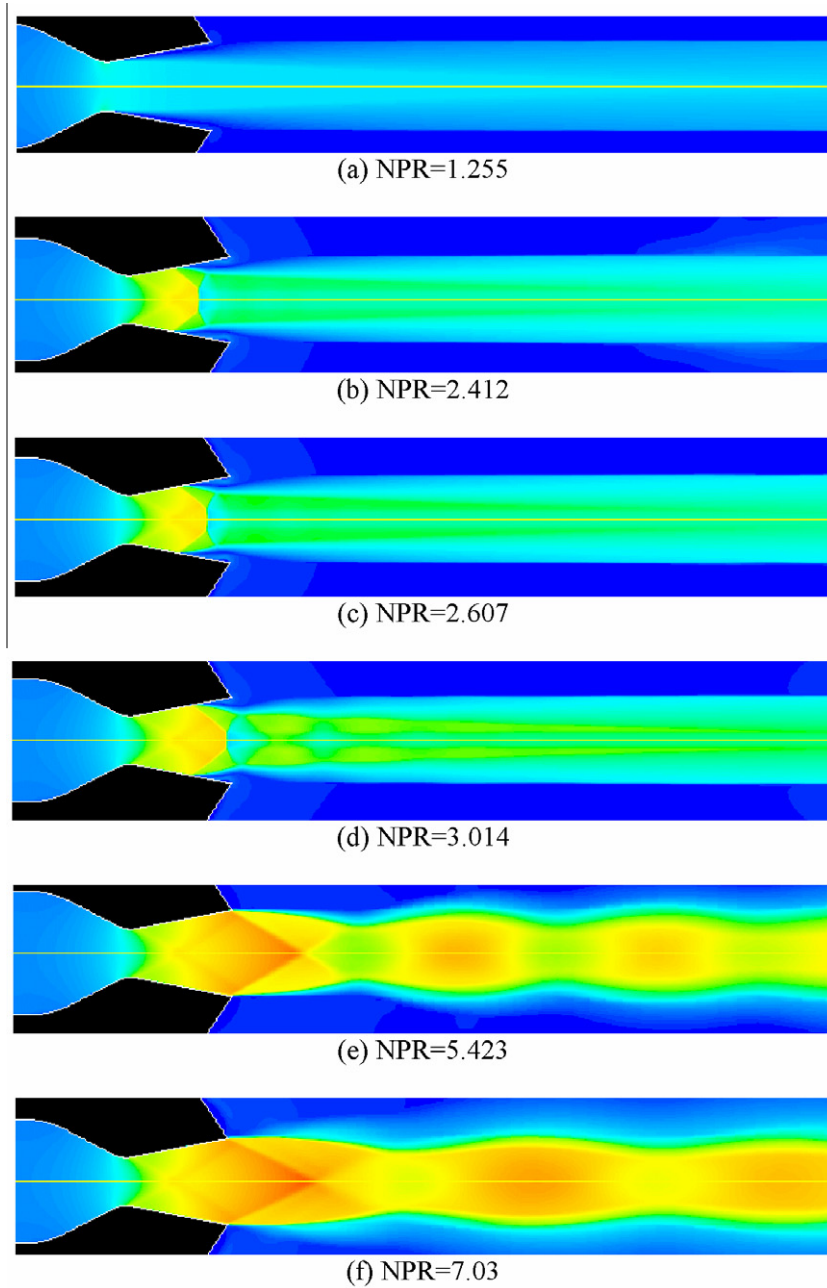


**Fig. 5.** The computed Mach number images for different nozzle pressure ratios.

The dimensionless shear stress ( $\tau/\tau_{in}$ ) distribution for different NPRs is plotted in Fig. 7, where  $\tau_{in}$  is the shear stress at the nozzle inlet. For separated flow at low NPR, the results indicate that the flow did not attach the nozzle surface and the free shear layer started at the trailing lambda foot is completely detaching past the shock. As the separation point become nearly near the effective nozzle exit, the lambda shock system adjusted to satisfy continuity of pressure and flow direction. This trend is indicated by a slight increase of the shear stress near the nozzle exit. These results can also be seen in the velocity vector graph, as shown in Fig. 8a, for  $NPR = 2.412$ , where a positive velocity distribution is obtained nearby the effective nozzle exit. By plotting the streamlines distribution, as shown in Fig. 8b, double eddy recirculation regions downstream of the flow separation point is observed. This can explain the existence of the positive values of wall shear stress near the nozzle exit.

The Mach contours, shown in Fig. 8c, illustrate the existence of lambda shock system which consists of a normal shock wave at the nozzle core and an oblique shock at the nozzle walls as a result of the boundary layer shock interaction.

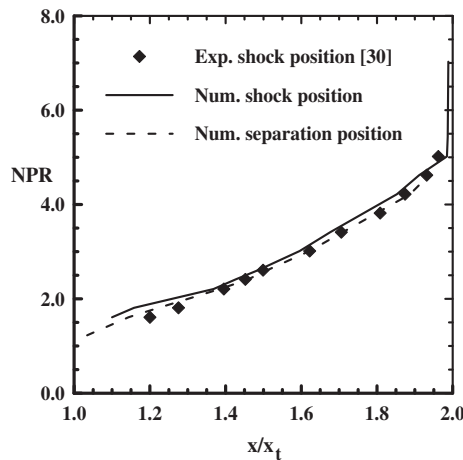


Fig. 6. Comparison of the predicted shock positions and the separation points locations.

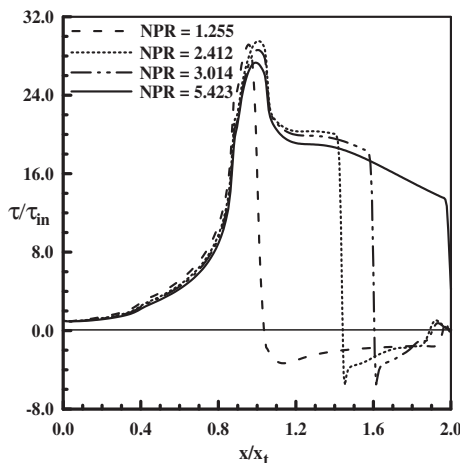


Fig. 7. The computed shear stress distribution at different NPRs.

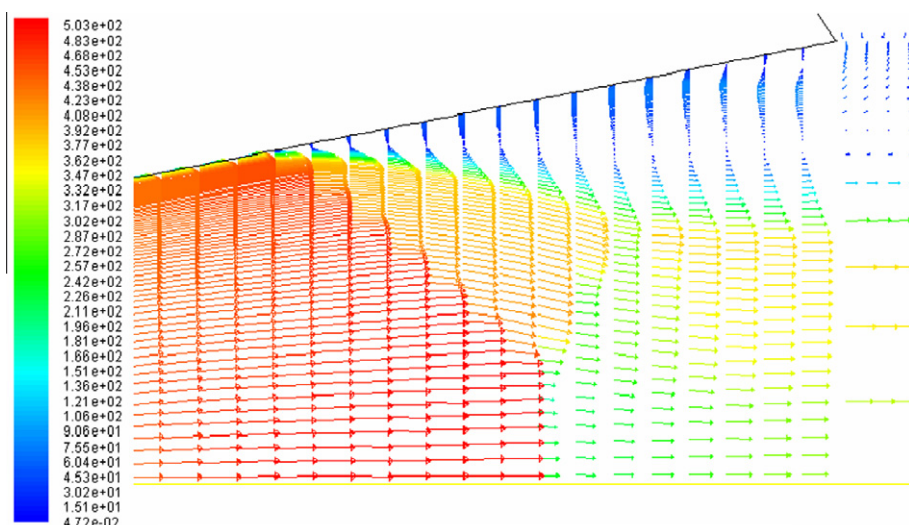
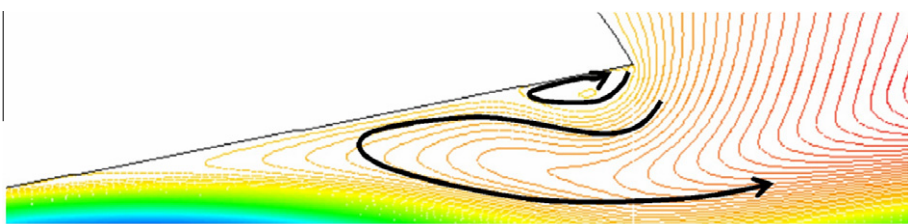
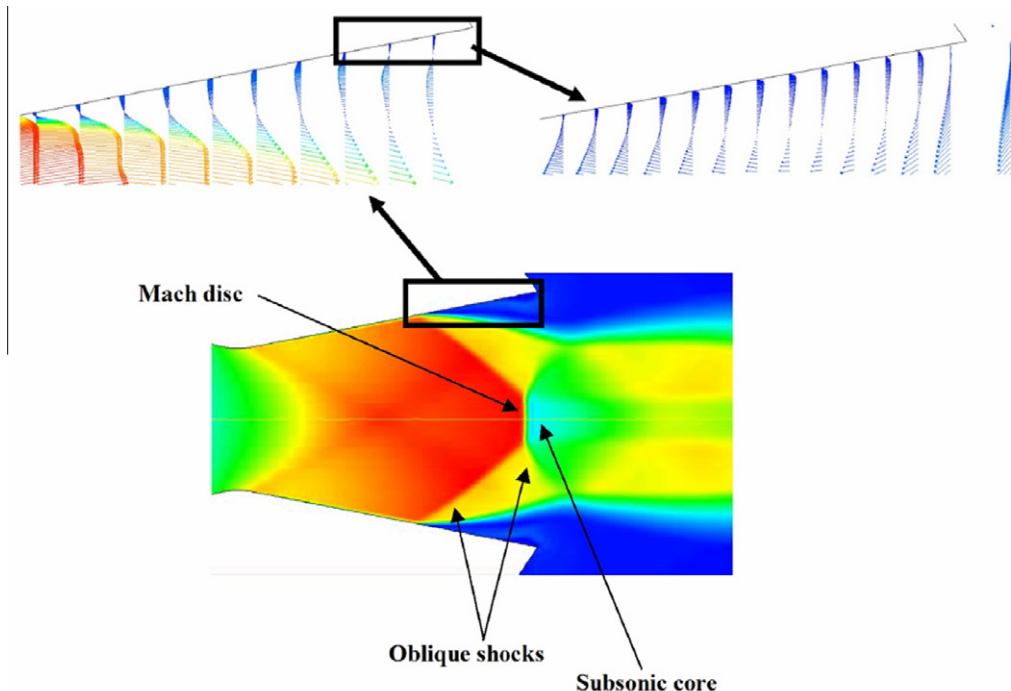


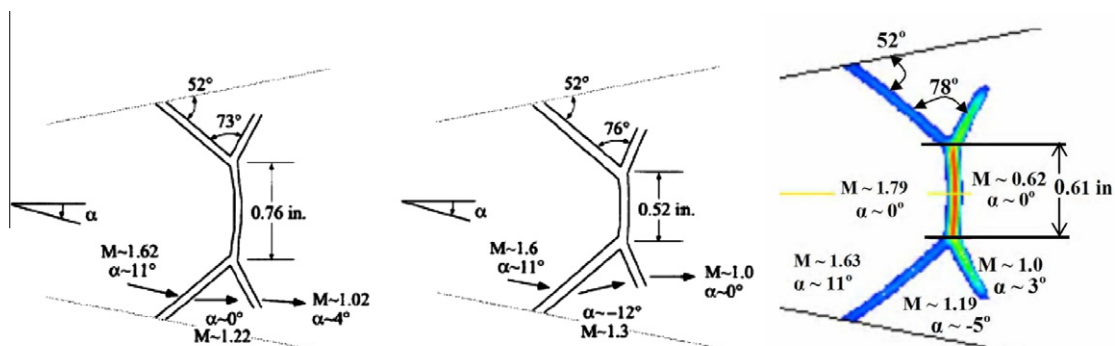
Fig. 8a. Velocity vector plot for  $NPR = 2.412$ .



**Fig. 8b.** Streamlines plot for  $NPR = 2.412$ .



**Fig. 8c.** Mach contours and velocity vector plot nearby nozzle exit for  $NPR = 2.412$ .



**Experimental Ref. [8]**

**Numerical Ref. [8]**

**Present computation**

**Fig. 9.** Comparison of the computational shock schematic, for  $NPR = 2.412$ , with previous experimental and numerical results [8].

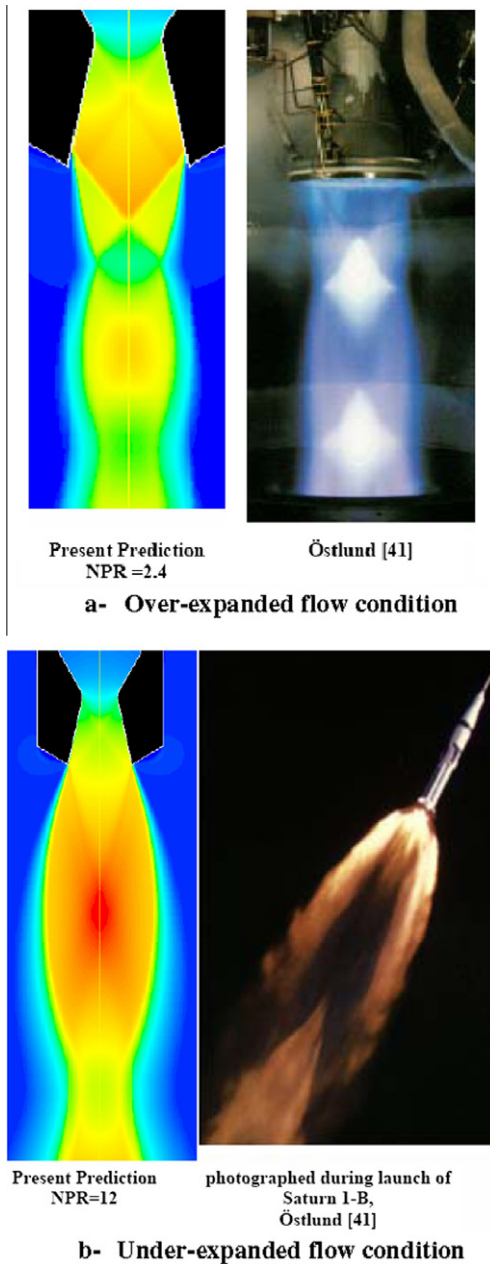


**Fig. 10.** Qualitative Comparison between predicted and observed flow pattern downstream nozzle exit.

Fig. 9 illustrates the computational shock schematic for  $NPR = 2.412$  compared with both the experimental measurement and the computational result of [8]. The present predicted shock height equals  $\approx 0.61$  in. Its value is located between the experimental measurements and the numerical results of [8], but closer to the experimental data than the previous numerical results of [8]. This comparison reveals the accuracy of the present numerical simulation performed.

As mentioned above, the exhaust flow pattern is dependent on whether the flow is over-expanded or under-expanded [20]. In an over-expanded flow conditions the ambient pressure is higher than the nozzle exit pressure, while for under-expanded flow conditions the ambient pressure is less than the nozzle exit pressure. In the case of over-expanded conditions, the exhaust flow adapts to the ambient through a system of oblique shocks and expansion waves. However, in the case of under expanded conditions, the exhaust gas continues its expansion behind the nozzle exit. Fig. 10 shows a good qualitative comparison between the present numerically predicted and the observed flow pattern downstream the nozzle exit for both flow conditions. The pictures used for the qualitative comparison are given in Ref. [41].

## 5. Conclusion

The numerical simulations of compressible flow passing through a 2D convergent–divergent nozzle with a fixed geometry and different nozzle pressure ratios are presented. The nozzle is assumed to have impermeable and adiabatic walls with a flow straightener in the upstream side and is connected to a plenum surrounding the nozzle geometry and extended in the downstream direction. The predicted results are obtained by solving the RANS equations for compressible flow in its conservative form coupled with both the energy equation and the equation of a state. Several turbulence models are applied, namely; the standard  $k-\varepsilon$  model, the extended  $k-\varepsilon$  model, shear-stress transport  $k-\omega$  model, Reynolds stress model,  $\nu^2-f$  model and the realizable  $\nu^2-f$  model. The numerical results reveal that, the SST  $k-\omega$  and the realizable  $\nu^2-f$  models give the best results compared with other models in predicting the shock wave position and the separation point, while other models give a poor prediction. The reason behind that may be related to the formulation of SST turbulence model in the gradual change from the standard  $k-\omega$  model in the inner region of the boundary layer to a high-Reynolds-number  $k-\varepsilon$  model in the outer part of the boundary layer. The  $\nu^2-f$  turbulence model incorporates some near-wall turbulence anisotropy as well as non-local pressure-strain effects, especially when the realizability constrains on the turbulent time scale is included which enhances greatly the prediction of the model for this particular case. However, the  $\nu^2-f$  has two extra transport equations as it compared with the SST model and therefore the computational time increases by about 20%. Furthermore, the low-Re SST model requires 4% computational time greater than the high-Re model. As a result, the high-Re SST turbulence model is recommended for nozzle flow problems. In more elaborated results, the comparison of the shock schematic with the previous numerical and experimental results show good and reasonable agreement with experimental measurements, which revealed the accuracy of the present computational methodology in predicting such phenomena.

## Acknowledgement

This work is financially supported by the Science and Technology Development Fund (STDF), Egypt, through the project STDF-ID-108.

## References

- [1] A. Ciucci, G. Iaccarino, R. Moser, F. Najjar, P. Durbin, Simulation of rocket motor internal flows with turbulent mass injection, Science, Center for turbulence research, in: Proceeding of the Summer Program, 1998, pp. 245–266.
- [2] A.M. Hegab, D.R. Kassoy, A.A. Sileem, Numerical investigation of acoustic-fluid dynamics interaction in an SRM chamber/nozzle model, in: 36th Aerospace Science Meeting, Reno, NV, USA, AIAA Paper 98-0712, 1998.
- [3] A. Hegab, Study of Acoustic Phenomena in a Solid Rocket Engines, Ph.D. Thesis, Mech. Power Engineering Dept., Menoufia Univ., Egypt, carried out at Center for Combustion Research, University of Colorado at Boulder, USA, 1998.
- [4] D.J. Dusa, Exhaust nozzle system design considerations for turbojet propulsion system, in: Proceedings of the 10th International Symposium on Airbreathing Engines, vol. 2, AIAA, Reston, VA, 1991, pp. 1100–1110.
- [5] A. Hegab, T. Jackson, J. Buckmaster, D. Stewart, Nonsteady burning of periodic sandwich propellants with complete coupling between the solid and gas phases, *J. Combust. Flame* 125 (2001) 1055–1070.
- [6] Q. Xiao, H.M. Tsai, D. Papamoschou, A. Johnson, Experimental and numerical study of jet mixing from a shock-containing nozzle, *J. Propulsion Power* 25 (2009) 688–696.
- [7] G.L. Romine, Nozzle flow separation, *AIAA J.* 36 (9) (1998) 1618–1625.
- [8] C.A. Hunter, Experimental, Theoretical and Computational Investigation of Separated Nozzle Flows, AIAA Paper 98-3107, 1998.
- [9] A. Zill, Flow separation in rectangular over-expanded supersonic nozzles, in: 44th AIAA Aerospace Science Meeting and Exhibit, Reno Nevada, 2006.
- [10] A.A. Khan, T.R. Shembharkar, Viscous flow analysis in a convergent–divergent nozzle, in: Proceedings of the International Conference on Aerospace Science and Technology, 26–28 June 2008, Bangalore, India.
- [11] D. Papamoschou, A. Zill, A. Johnso, Supersonic flow separation in planar nozzles, *Shock Waves* 19 (2009) 171–183.
- [12] Q. Xiao, H.M. Tsai, Numerical investigation of supersonic nozzle flow separation, *AIAA J.* 45 (2007) 532–541.
- [13] T. Gawehn, A. Gühan, N.S. Al-Hasan, G.H. Schnerr, Experimental and numerical analysis of the structure of pseudo-shock systems in Laval nozzles with parallel side walls, *Shock Waves* 20 (2010) 297–306.
- [14] S.C. Gikley, R.H. Hines, R.J. Shaw, Installing a propulsion system in the HSCT, *Mech. Eng.* 117 (8) (1995) 98–101.
- [15] A. Johnson, D. Papamoschou, Shock motion and flow instabilities in supersonic nozzle flow separation, in: 38th Fluid Dynamics Conference and Exhibit, Washington, 2008.
- [16] W. ElAskary, A. Balabel, Prediction of reattaching turbulent shear flow in asymmetric divergent channel using linear and non-linear turbulence models, *Eng. Res. J. (ERJ)*, Faculty of Eng., Menoufia Univ. 30 (4) (2007) 535–550.
- [17] A. Balabel, RANS modeling of gas jet impinging onto a deformable liquid interface, *Emirates J. Eng. Res. (EJER)* 12 (3) (2007) 35–46.
- [18] A. Hegab, W.A. El-Askary, A. Balabel, S.M. El-Behey, RANS simulation of turbulence in a porous channel with constant mass injection, in: Proceedings of the 13th International Conference Aerospace Science & Aviation Technology, ASAT, 2009.
- [19] A. Hamed, C. Vogiatzis, Overexpanded two-dimensional convergent–divergent nozzle flow simulations, assessment of turbulence models, *J. Propulsion Power* 13 (1997) 444–445.
- [20] A. Hamed, C. Vogiatzis, Overexpanded two-dimensional convergent–divergent nozzle performance, effects of three-dimensional flow interactions, *J. Propulsion Power* 14 (2) (1998) 234–240.
- [21] A. Hamed, C. Vogiatzis, Three-Dimensional Flow Computations and Thrust Predictions in 2DCD Overexpanded Nozzles, AIAA Paper 97-0030, 1997.
- [22] K.J. Plotkin, Shock wave oscillation driven by turbulent boundary layer fluctuations, *AIAA J.* 13 (8) (1975) 1036–1040.
- [23] J.P. Dussauge, P. Dupont, J.F. debieve, Unsteadiness in shock wave boundary layer interaction with separation, *Aerosp. Sci. Technol.* 10 (2) (2006) 85–91.
- [24] A. Bourgoing, Ph. Reijasse, Experimental analysis of unsteady separated flows in a supersonic planar nozzle, *Shock Waves* 14 (4) (2005) 251–258.
- [25] S.V. Patankar, Numerical Heat Transfer and Fluid Flow, McGraw Hill, New York, 1980.
- [26] B.E. Launder, D.B. Spalding, Mathematical Models of Turbulence, Academic, London, 1972, pp. 169–189.
- [27] Y.S. Chen, S.W. Kim, Computation of Turbulent Flows using Extended  $k-\varepsilon$  Turbulence Closure Model, NASA CR-179204, 1987.
- [28] F.-S. Lien, G. Kalitzin, Computations of transonic flow with the  $\nu^2-f$  turbulence model, *Int. J. Heat Fluid Flow* 22 (2001) 5361.
- [29] P.A. Durbin, On the  $k-\varepsilon$  stagnation point anomaly, *Int. J. Heat Fluid Flow* 17 (1995) 89–90.

- [30] F.R. Menter, Two-equation eddy-viscosity turbulence models for engineering applications, *AIAA J.* 32 (1994) 1598–1605.
- [31] Fluent, User's Guide Fluent 6.3.26, Fluent Incorporated, Lebanon, NH, 2006.
- [32] B.E. Launder, D.B. Spalding, Mathematical Models of Turbulence, Lectures Notes, Imperial College of Science and Technology, London, England, 1972.
- [33] A. Svenningsson, L. Davidson, Assessment of realizability constraints in  $v^2-f$  turbulence models, *Int. J. Heat Fluid Flow* 25 (2004) 785–794.
- [34] B.E. Launder, D.P. Spalding, The numerical computation of turbulent flows, *Comput. Methods Appl. Mech. Eng.* 3 (1974) 269–289.
- [35] S.E. Kim, D. Choudhury, A Near-Wall Treatment using Wall Functions Sensitized to Pressure Gradient, ASME FED, Separated and Complex Flows, vol. 217, ASME, 1995.
- [36] G. Iaccarino, Predictions of a turbulent separated flow using commercial CFD codes, *Trans. ASME, J. Fluids Eng.* 123 (2001) 819–828.
- [37] S.M. El-Behery, M.H. Hamed, A comparative study of turbulence models performance for turbulent flow in a plane asymmetric diffuser, *Int. J. Aerosp. Mech. Eng.* 5 (2011) 78–89.
- [38] S. Etemad, B. Sundén, Numerical investigation of turbulent heat transfer in a rectangular-sectioned 90° bend, *Numer. Heat Transfer, Part A* 49 (2006) 323–343.
- [39] J. Östlund, Assessment of Turbulence Models in over Expanded Rocket Nozzle Flow Simulation, AIAA Paper 99-2583.
- [40] F.R. Menter, M. Kuntz, R. Langtry, Ten years of industrial experience with the SST turbulence model, in: K. Hanjalic, Y. Nagano, M. Tummers (Eds.), *Turbulence, Heat and Mass Transfer*, vol. 4, Begell House Inc., 2003, pp. 625–632.
- [41] J. Östlund, Flow Processes in Rocket Engine Nozzles with Focus on Flow Separation and Side-loads, TRITA-MEK, Technical Report 2002:09, Licentiate Thesis, Royal Inst. of Tech., Stockholm, 2002.